Mechanical evaluation of a patient-specific additively manufactured subperiosteal jaw implant (AMSJI) using finite element analysis

Eline De Moor[1], Stijn E.F. Huys[1], G. Harry van Lenthe[1], Maurice Y. Mommaerts[2], Jos Vander Sloten[1]

[1]*Department of Mechanical Engineering, Biomechanics section, KU Leuven, Leuven, Belgium*

[2]*European Face Centre, Universitair Ziekenhuis Brussel, VUB, Brussels, Belgium*

Corresponding author: Maurice Yves Mommaerts

European Face Centre, Universitair Ziekenhuis Brussel, Vrije Universiteit Brussel

Laarbeeklaan 101

1090 Brussels

Belgium

e-mail: mauricemommaerts@me.com

Grants: The resources and services used in this work were provided by the VSC (Flemish Supercomputer Center) and funded by the Research Foundation - Flanders (FWO) and the Flemish Government.

Key-words: patient-specific modeling; protheses and implants; mouth, edentulous; atrophy.

Abstract

Edentulism with associated severe bone loss is a widespread condition that hinders the use of common dental implants. An additively manufactured subperiosteal jaw implant (AMSJI) was designed as an alternative solution for edentulous patients with Cawood and Howell class V-VIII bone atrophy. A biomechanical evaluation of this AMSJI for the maxilla in a Cawood and Howell class V patient was performed via finite element analysis. Occlusal and bruxism forces were incorporated to assess the loading conditions in the mouth during daily activities. The results revealed a safe performance of the implant structure during the foreseen implantation period of 15 years when exerting average occlusion forces of 200 N. For the deteriorated state of class VIII bone atrophy, increased stresses on the AMSJI were evaluated, which predicted implant fatigue. In addition, excessive bruxism and maximal occlusion forces might induce implant failure due to fatigue. The models predicted bone ingrowth at the implant scaffolds, resulting in extra stability and secondary fixation. For all considered loading conditions, the maximal stresses were located at the AMSJI arms. This area is most sensitive to bending forces and hence, allows for further design optimization. Finally, the implant is considered safe for normal daily occlusion activities.

Edentulism is a major disease worldwide, with a high prevalence in elderly patients[1,2]. The complete and irreversible loss of natural teeth has a significant impact on the health status of patients, causing functional and social limitations[2]. Patients with healthy maxillary bone qualify for root-shaped implants with associated dentures. Solutions for patients with excessive bone atrophy include bone grafting with the placement of root-shaped implants, the All-on-4 concept, quad-zygoma implants or combinations. Bone grafting has potential complications including nerve injury, hematoma, fracture, infection, bone loss and oroantral fistulation[3]. Single implant loss after All-on-4 results in a critical end-stage situation[4]. Disadvantages of zygomatic implants include the need for excellent surgical skills because piercing the Schneiderian membrane of the maxillary sinus should be prevented[5]. In addition, complications such as infection at the implant tip, tissue retraction, communication between the oral cavity and the maxillary sinus, extraoral fistulation and intra-orbital abscesses can occur[5]. The Additively Manufactured Subperiosteal Jaw Implant (AMSJI) poses an alternative[6,7]. The implant is designed for patients with Cawood and Howell class V-VIII maxillary bone atrophy. This patient-specific design is three-dimensionally (3D) printed using TiAl6V4 grade 23 Extra Low Interstitial (ELI). The AMSJI-concept consists of three components: a left and right AMSJI subunit and an intra-oral connector. The AMSJI subunits are placed subperiosteally, while the connector (supra-structure) links them together. Both AMSJIs are provided with a scaffold region at the bone-implant interface to sustain and support tissue ingrowth and stabilization of the implant[7,8]. Figure 1 shows a left AMSJI segment with indicated color-coded components. Two wings (red) make a connection with the basal looped frame (orange). The arms (green) are the connection between the basal looped frame and the posts (yellow). In the wings, holes are present for placing osteosynthesis screws. The division into subparts improves the procedure for both surgeon and patient. The patient will experience less pain and edema because the incision wounds are smaller. In addition, the surgeon will experience more comfort while performing the operation, which is usually done using local anesthesia, nasotracheal intubation, or intravenous sedation.

The purpose of this study was to perform a biomechanical evaluation of the revisited subperiosteal implant concept, using finite element analysis (FEA) subjected to the physiological and pathological loading conditions in the mouth, to provide clinically relevant information about failure and fatigue of the implant structure, stress shielding of the bone tissue, and the effects of osseointegration in the scaffolds.

2. Materials and Methods

Segmentation of Digital Imaging and Communications in Medicine (DICOM) images with Mimics Innovation Suite 22 was performed on CT scans for the implants, which were designed using Geomagics Sculpt 2019.2.50 (3D Systems). This resulted in surface tessellation language (STL) files of the maxillofacial complex designed by CADskills. Autodesk Meshmixer 3.5.474 and Materialise 3-matic 14.0 were used to process and remesh the parts, respectively, using C3D10M mesh elements. A convergence study was performed to determine an appropriate mesh density, taking the tradeoff between the accuracy of the results and the computational load into account. A mesh density was chosen for which the average von Mises stress values did not deviate more than 4.4% from the converged value. Two different meshes were created, one for a Cawood and Howell class V patient and one for a Cawood and Howell class VIII patient. In the latter, the maxillary component was further resorbed based on the first mesh using Autodesk Meshmixer. The volume meshes were exported to the FEA software Abaqus/CAE 2017. Table 1 shows the different material properties assigned to the different components in the assembly. All materials were assumed to be linear elastic and isotropic. Titanium Grade 23 (TiAl6V4) ELI was used for both AMSJI subunits and the connector, with yield strength σ_y = 1116 MPa and ultimate strength σ_t = 1286 MPa (Table 1).

In addition, material properties of cortical bone tissue were applied for the maxilla. The scaffolds consisted of diamond unit cells with 500 µm pores with a porosity P of 80%.

Immediately after surgery, the scaffold was assumed to be filled with body fluids. The following formula was used to obtain the Young's modulus E of an open cellular structure or scaffold: $E = E_0 (\frac{\rho}{\rho_0})^2$, where E_0, ρ and ρ_0 are the Young's modulus of the fully dense material, the corresponding porous material density and the corresponding fully dense material density, respectively[9,10]. In addition, the relationship between the Poisson's ratio and the relative density of the open cell structures was used to estimate the Poisson's ratio of the scaffold[11]. Four different loading conditions were considered in order to mimic the daily activity in the mouth. A force of 200 N was applied to the molar region on the left side of the mouth in the case of average occlusion. For maximum occlusion, 1000 N was assumed. Directions of the force were corrected in all three dimensions, taking into account the inclination of the molar cusps. In addition, both clenching and grinding loading conditions were considered. Clenching forces of 1000 N were applied in the vertical direction over the whole connector, whereas grinding forces of 500 N were considered horizontally and unilaterally in the molar region. Movement of the maxilla was restricted by applying a boundary condition to its upper edge. Appropriate contact interactions in both normal and tangential directions were defined between the different parts of the assembly. The Coulomb friction model was used for the tangential component, with a friction coefficient of 0.36 and 0.30 for titanium-titanium and titanium-bone, respectively[11,12].

Furthermore, the scaffolds were tied to the implant. No friction was assumed between the scaffolds and the AMSJIs. The maximum stresses in the FEA models were calculated as the average of the magnitudes in the nodes of the element experiencing the highest stresses and were defined as the average peak stress. This was done to avoid the contribution of unreliable outlier values.

3. Results

3.1. Average occlusal forces

For an average occlusal load of 200 N applied to the left side of the mouth, the maximum von Mises stress was reached in the left AMSJI, as shown in Figure 2. For the average occlusion model, the average peak stress was located at the middle arm and equaled 178.8 MPa. The logarithmic strains in the maxilla are shown in Figure 3. Microstrains lower than the threshold of 50 με are shown in black. A few nodes exceeded the upper threshold of 1500 με. The highest logarithmic strains were located at the upper edge of the maxilla, indicated in gray in Figure 3.

3.2. Maximal occlusal forces

In the case of maximal occlusal forces of 1000 N, the average peak von Mises stress located at the middle arm of the left AMSJI increased to 902.0 MPa. Figure 4 shows the microstrains in the maxilla when experiencing maximal occlusion. Higher values were present, reaching up to 7000 με. In addition, Table 2 gives the relative micromotions between the scaffolds and the bone tissue in all three directions.

3.3. Maximal clenching forces

Clenching forces of 1000 N on both sides of the mouth resulted in maximum von Mises stresses on the left AMSJI, as shown in Figure 5. The average peak value equaled 420.8 MPa and was located at the medial arm. Logarithmic strains in the maxilla showed a similar pattern as the strain distribution of the average occlusion case. Except for the higher values at the upper edge of the maxilla, microstrains did not exceed 1500 με.

3.4. Maximal grinding forces

Figure 6 shows von Mises stresses on the implant structure in the case of 500 N unilateral grinding. The highest von Mises stresses were located at the middle and lateral arm of the left AMSJI. The maximal average peak stress equaled 638.7 MPa. Figure 7 shows the logarithmic strains in the maxilla. Values up to 4000 με were reached.

3.5. Class V and class VIII comparison

After further bone resorption at the residual ridge, the average peak von Mises stress in the left AMSJI, located at the middle arm, increased to 201.5 MPa. The order of magnitude of the microstrains in the maxilla of the class VIII patient did not change compared to the class V patient.

4. Discussion

The implant structure will be subjected to various loading conditions during normal daily activities. Numerous studies have investigated the values of forces applied on the teeth during mastication[13-17]. However, these studies report a wide variation of force magnitudes, which can be explained by both the inherent variability of the mastication process and the use of various measurement methods[13]. In the literature, the voluntary bite forces in healthy dentate subjects reach diverging values ranging from 70 N up to 1000 N in maximal occlusion cases[13,17-20]. These bite forces are applied on the teeth in an intermittent, rhythmic, and dynamic way with an average total time of 1050 s or 17 min 30 s per day (24 h)[21]. Most studies only consider the vertical bite forces, but in theory, bite forces might be exerted in all three dimensions[14]. The non-perpendicular components of the occlusion forces can provide a significant contribution to the loading pattern exerted on the teeth and jaw[13,14]. Chewing on a food bolus usually takes place in the posterior region and alternates between the left and right sides of the mouth, more specifically in the region covered by the canines, premolars, and molars. In addition, the jaw muscles may also exert forces unrelated to the processing of food. Bruxism is defined as the involuntary rhythmic or spasmodic clenching or grinding of teeth[22]. Clenching refers to the pressing and clamping of the teeth together, which is often associated with acute nervous tension[22]. On the other hand, grinding is defined as the act of correcting occlusal disharmonies by grinding the natural or artificial teeth[22]. As is the case for voluntary occlusal forces, bruxism forces reach a broad range of values of 1000 N or even higher[23-25].

For all considered loading patterns, the average peak value stresses experienced by the implant structure were lower than both the yield and ultimate strength of TiAl6V4 grade 23 ELI. Thus, no plastic deformation or immediate fracture of the implant is expected. However, in the case of maximal occlusion of 1000 N, the maximal stress approached the yield strength of 1116 MPa in some individual nodes of the AMSJI arms, which increases the risk of plastic deformation.

It is recommended to avoid maximal voluntary occlusion as much as possible when wearing the implant structure. Attention should be paid to patients wearing both upper and lower implants. Due to the loss of their proprioception, higher occlusion forces might be exerted, leading to plastic deformation and failure of the AMSJI structure. In addition, extra simulations of the denture structure revealed no fracture of the denture when experiencing maximal occlusion or grinding forces. Thus, a denture fracture is not expected to occur before the AMSJIs experience risky stress conditions.

In order to predict whether the implant structure will survive the foreseen implantation period, the fatigue properties of the implant structure were considered. For a planned period of 15 years and assuming a total of 1050 chewing cycles per 24 h[21], a fatigue threshold of approximately 200 MPa was defined, taking into account the manufacturing process, the surface roughness, and the heat treatment of the titanium-alloy[26]. In the case of average occlusion, the average peak stresses were lower than the predefined fatigue threshold of 200 MPa and hence, the implant is expected to withstand the applied forces during the planned 15 years. However, in the case where the bone further resorbed after placement of the implant structure, the average peak stress equaled 201.5 MPa and approached the fatigue threshold. As a result, fatigue is expected to occur for the titanium implants, initiating localized plastic deformation, cracks, or even failure[27]. Therefore, practitioners should monitor for possible further bone resorption.

Even if adequate stresses and strains are transmitted to the alveolar ridge, which avoids the occurrence of disuse atrophy, further residual ridge resorption (RRR) is not completely excluded. Other biological processes might induce important contributions to the RRR and

should not be neglected. Further investigation of the RRR processes is necessary. For maximal occlusion, the fatigue thresholds for clenching and grinding forces should be determined depending on the total number of cycles of these events. However, due to the patient-specific nature of bruxism, no consensus exists in the literature. Inverse calculations predict that the implant can only withstand a maximum of seven clenching events per 24 h in order to avoid fatigue. In the case of grinding, only one event per 24 h is allowed. These results indicate the danger of inserting an AMSJI in bruxists. As a result, it is recommended to exclude bruxism patients from the target group of AMSJI.

The abovementioned results should be treated with caution for the following reasons. First, the applied forces are considered maximal 'worst cases'. The magnitude of the forces is expected to be lower in reality. Secondly, in the real-life situation, the magnitude of occlusal and bruxism forces will differ from cycle to cycle, which can influence the fatigue results. Finally, some assumptions were made regarding the manufacturing process, heat treatment, and surface quality of the AMSJI, which also affect the fatigue threshold.

The bone physiology and the occurrence of stress shielding were investigated via microstrains experienced by the maxilla. Microstrains in the range of 50 to 1500 με represent a steady state of the bone tissue, without net changes in the bone volume[28,29]. Disuse atrophy or stress shielding was expected to occur for values lower than 50 με, whereas values exceeding 1500 με indicated overload on the bone tissue. Mild overload results in net bone growth, whereas pathological overload will result in a net loss of bone volume[28,29]. For average occlusion and clenching, the magnitude of the microstrains remained in the physiological range, indicating that no stress-shielding and no net bone growth is expected. As indicated in Figure 3 by the black colors, resorption of some bony protrusions is expected in the case of average occlusion due to microstrains lower than 50 με. However, it is not expected that resorption of these protuberances will lead to further stress shielding with associated bone loss of the overall alveolar ridge. In fact, according to the results, the load transfer at the implant-bone interface

and the corresponding microstrains were still adequate in the region of the alveolar ridge to prevent further resorption. Furthermore, several increased values were seen at particular nodes and elements located at the interface of the maxilla and the AMSJIs. However, it was assumed that these restricted strain concentrations were caused by poor contact interactions and therefore, they were disregarded. In addition, the higher microstrains at the upper edge of the maxilla corresponded to the region of the applied boundary conditions. Hence, these values were also considered unreliable. Figure 4 shows the microstrains in the case of unilateral maximal occlusion. The results indicated an overload of the bone tissue with corresponding changes in the bone remodeling process. Similar results were obtained for the microstrains when exerting unilateral grinding forces. Again, the results predict dangerous consequences for both maximum occlusion forces and grinding forces, emphasizing the need to avoid these forces as much as possible in AMSJI-wearing patients.

The relative motions between the bone and the scaffolds were tested for the extreme occlusion case. All relative motions were lower than 28 µm, which is the threshold value for maximal motions between both scaffold and bone in order to ensure bone ingrowth[30,31]. As a result, osseointegration is expected to occur when exerting both maximal and average occlusal forces. The resulting bone ingrowth ensures extra stability of the implant and thus secondary fixation.

Finally, the results show that the arms experienced higher stresses than the rest of the implant for all tested loading conditions. In addition, a sensitivity analysis revealed increasing maximal stresses on the AMSJI when the vertical inclination angle increased. This implies that the arms are sensitive to bending forces. Therefore, this region can be considered the weakest spot of the AMSJI. Lateral forces should be avoided as much as possible in AMSJI-wearing patients. However, the slope of natural teeth, which was used during the simulations, is often higher than the slope of the molars in dentures. Due to the flatter cusps of the molars in dentures, the contribution of the lateral forces will be lower, which diminishes the lateral contribution to the

implant structure. This will lead to smaller bending moments experienced by the AMSJI arms and thus have a beneficial effect.

5. Conclusion

The FEA simulations predicted a stable and safe implementation of AMSJI for class V patients exerting average occlusal forces during daily activity. However, further resorption of the residual ridge might cause fatigue of the implant. It is recommended to follow-up regarding the quality of the bone after placement of the AMSJIs. Furthermore, fatigue of the implant is a potential risk for bruxism patients and therefore, it is advisable to exclude bruxism patients from the target group for AMSJI. Maximum and exaggerated voluntary occlusion forces should be avoided because in extreme situations, they can induce plastic deformation of the implant and consequently lead to a fracture. For all considered loading cases, the highest stresses in the AMSJIs were located at the arms, which are sensitive to bending forces. Optimization of the current design could include the strengthening of the arms to improve the safety of the implant structure. Finally, under normal circumstances, the AMSJI design is completely safe to use and considered the best solution for edentulous patients with Cawood and Howell class V-VIII bone resorption.

Funding

The resources and services used in this work were provided by the VSC (Flemish Supercomputer Center) and funded by the Research Foundation - Flanders (FWO) and the Flemish Government.

Acknowledgments

Special thanks to CADskills: Benoit de Smet (Product Manager AMSJI) for providing the materials and data necessary for this project.

Interest disclosure

Prof. Maurice Mommaerts is Innovation Manager and Statutory Manager at CADskills. Drs. ir. Stijn Huys is R&D Officer and Quality Manager in the same company.

References

1. Sanders AE, Slade GD, Carter KD, Stewart JF. Trends in prevalence of complete tooth loss among Australians, 1979-2002. Aust N Z J Public Health 2004;28:549–554. doi: 10.1111/j.1467-842x.2004.tb00045.x.

2. Emami E, Freitas de Souza R, Kabawat M, Feine JS. Review article: The impact of edentulism on oral and general health. Int J Dent 2013;2013:1–7. doi: 10.1155/2013/498305.

3. Myeroff C, Archdeacon M. Autogenous bone graft: donor sites and techniques. J Bone Joint Surg Am 2011;93;2227–2236. doi: 10.2106/JBJS.J.01513.

4. Chan MH, Holmes C. Contemporary 'All-on-4' concept. Dent Clin North Am 2015;59:421–470. doi: 10.1016/j.cden.2014.12.001.

5. Davo R, David L. Quad zygoma technique and realities. Oral Maxillofac Surg Clinics North Am 2019;31:285–297. doi: 10.1016/j.coms.2018.12.006.

6. Mommaerts MY. Additively manufactured sub-periosteal jaw im-plants. Int J Oral Maxillofac Surg 2017;46: 938–940. doi: 10.1016/j.ijom.2017.02.002.

7. Mommaerts MY. Evolutionary steps in the design and biofunctionalization of the additively manufactured sub-periosteal jaw implant 'AMSJI' for the maxilla. Int J Oral Maxillofac Surg 2019;48:108–114. doi: 10.1016/j.ijom.2018.08.001.

8. van den Dolder J, Jansen JA. Titanium Fiber Mesh: A Non-degradable Scaffold Material. In: Bronner F, Farach-Carson MC Mikos AG (eds.), Engineering of Functional Skeletal Tissues, Volume 3 in the Series Topics in Bone Biology. London: Springer-Verlag London Limited, 2007:69–80.

9. Gibson L, Ashby MF. Cellular Solids: Structure and Properties. New York: Cambridge University Press, 1997:528.

10. Murr LE, Gaytan SM, Medina F, Lopez H, Martinez E, Machado BI, Hernandez DH, Martinez L, Lopez MI, Wicker RB, Bracke J. Next-generation biomedical implants using additive manufacturing of complex, cellular and functional mesh arrays. Phil Trans R Soc A 2010;368;1999–2032. doi: 10.1098/rsta.2010.0010.

11. Zadpoor AA, Hedayati R. Analytical relationships for prediction of the mechanical properties of additively manufactured porous biomaterials. J Biomed Mater Res. Part A 2016:1–11. doi: 10.1002/jbm.a.35855.

12. Ramos AM, Mesnard M. The stock alloplastic temporo-mandibular joint implant can influence the behavior of the opposite native joint: A numerical study. J Craniomaxillofac Surg 2015;43:1384–1391. doi: 10.1016/j.jcms.2015.06.042.

13. Las Casas EB, de Almeida AF, Cimini Junior CA, de Tarso Vida Gomes P, Cornacchia TPM, Saffar JME. Determination of tangential and normal components of oral forces. J Appl Oral Sci 2007;15:70–76. DOI: 10.1590/s1678-77572007000100015

14. van Eijden TM. Three-dimensional analyses of human bite-force magnitude and moment. Arch Oral Biol 1991;36:535–539. DOI: 10.1016/0003-9969(91)90148-n

15. Gibbs CH, Mahan PE, Lundeen HC, Brehnan K, Walsh EK, Holbrook WB. Occlusal forces during chewing and swallowing as measured by sound transmission. J Prosthet Dent 1981;46:443–449. doi: 10.1016/0022-3913(81)90455-8.

16. Howell AH, Brudevold F. Vertical forces used during chewing of food. J Dent Res 1950;29;133–136. DOI: 10.1177/00220345500290020401

17. Taylor A, Yuan T, Ross CF, Vinyard CJ. Jaw-muscle force and excursion scale with negative allometry in platyrrhine primates. Am J Phys Anthropol 2015;158:242–256. DOI: 10.1002/ajpa.22782

18. Trulsson M. Force encoding by human periodontal mechanoreceptors during mastication. Arch Oral Biol 2007;52:357–360. doi: 10.1016/j.archoralbio.2006.09.011.

19. Dong-Soon C, Bong-Kuen C, Insan J, Kyung-Hwa K, Sang-Cheol K. Three-dimensional finite element analysis of occlusal stress distribution in the human skull with premolar extraction. Angle Orthod 2013;83:204–211. doi.org/10.2319/020112-89.1

20. Trojan L, Gonzalez Torres LA, de Freitas Pinto RLU, Melo AC, Las Casas EB. Maxillary biomechanical study during rapid expansion treatment with simplified model. J of Medical Imaging Health Inform 2014;4:1–5. DOI: 10.1166/jmihi.2014.1233

21. Zarb GA, Hobrink J, Eckert S, Jacob R. Prosthodontic Treatment for Edentulous Patients: Complete Dentures and Implant-Supported Prostheses, thirteenth edition ed. Missouri: Elsevier Mosby, 2013:7–8.

22. Ferro KJ, Morgano SM, Driscoll CF, Freilich MA, Guckes AD, Knoernschild KL, McGarry TJ. The glossary of prosthodontic terms: 9th edition. J Prosthet Dent, 2017;117(5S), e1–e105.

23. Gibbs CH, Anusavice KJ, Young HM, Jones JS, Esquivel-Upshaw JF. Maximum clenching force of patients with moderate loss of posterior tooth support: A pilot study. J Prosthet Dent 2002;88:498–502. doi: 10.1067/mpr.2002.129062.

24. Nishigawa K, Bando E, Nakano M. Quantitative study of bite force during sleep associated bruxism. J Oral Rehab 2001;28:485–491. doi: 10.1046/j.1365-2842.2001.00692.x.

25. de Brito Sanchez R, de Melo Setter C, Corrêa Rodrigues J, Valladão Oliveira de Mello J, Arnaldo dos Santos Junior J, Martini Rodrigues SC, Matos da Silva Boschi SR, Scardovelli TA, Pereira da Silva A. Device for Evaluating the Bite Force of Night Bruxism, In: Costa-Felix R, Machado J, Alvarenga A (eds) XXVI Brazilian Congress on

Biomedical Engineering. IFMBE Proceedings, vol 70/1. Singapore: Springer, 2019. https://doi.org/10.1007/978-981-13-2119-1_68

26. Greitemeier D, Palm F, Syassen F, Melz T. Fatigue performance of additive manufactured tial6v4 using electron and laser beam melting. Int J Fatigue 2017;94:211–217. DOI: 10.1016/j.ijfatigue.2016.05.001

27. Lee YL, Barkey ME, Kang HT. Metal Fatigue Analysis Handbook. Practical problem-solving techniques for computer-aided engineering. Oxford: Butterworth-Heinemann, 2012:61–87.

28. Misch CE. Dental Implant Prosthetics. Mosby, 2005:132–133.

29. Resnik RR. Misch's Contemporary Implant Dentistry, 4th edition, Mosby - Elsevier, 2020: 451–453.

30. Pilliar RM, Lee JM, Maniatopoulos C. Observations on the effect of movement on bone ingrowth into porous-surfaced implants. Clin Orthop Relat Res 1986: 208:108–113.

31. Huang HL, Su KC, Fuh LJ, Chen MYC, Wu J, Tsai MT, Hsu JT. Biomechanical analysis of a temporomandibular joint condylar prosthesis during various clenching tasks. J Craniomaxillofac Surg 2015;43:1194–1201. DOI: 10.1016/j.jcms.2015.04.016

32. Azo materials. Grade 23 Ti 6Al 4V ELI alloy (UNS R56401), https://www.azom.com/article.aspx?ArticleID=9365, 2015, [Accessed: 23.10.2020].

33. SLM Solutions GmbH: Material Data Sheet Ti6Al4V(grade23)/3.7175/F136, 1–4, 2015.

34. Peterson J, Wang Q, Dechow PC. Material properties of the dentate maxilla. Anat Rec 2006;288A:962–972. doi: 10.1002/ar.21124.

35. Lai YS, Huang CH, Chen WC, Cheng CK. The effect of graft strength on knee laxity and graft in-situ forces after posterior cruciate ligament reconstruction. PLoS ONE 2015;10:1–11. DOI: 10.1371/journal.pone.0127293

36. Seong WJ, Kim UK, Swift JQ, Heo YC, Hodges JS, Ko CC. Elastic properties and apparent density of human edentulous maxilla and mandible. Int J Oral Maxillofac Surg 2009;38:1088–1093. DOI: 10.1016/j.ijom.2009.06.025

Tables

Table 1 Material properties

Material	E (GPa)	ν
TiAl6V4[32,33]	111	0.34
Bone[34-36]	15	0.3
Scaffold (no osseointegration) [9,11]	4.4	0.43

Legends: E: Young elastic modulus; ν: Poisson ratio

Table 2 Relative motions between the scaffolds and the bone tissue

	Avg. L (μm)	Avg. R (μm)	Max. L/R (μm)
Contact opening	5.83	3.00	15.96
Tangential motion (x)	0.14	0.0041	16.18
Tangential motion (y)	0.021	0.0061	8.47

Abbreviations: Avg.: average; Max.: maximum

Table 3 Maximum stresses (MPa) in the implant structure

	1. (MPa)	2. (MPa)	3. (MPa)	4. (MPa)
Grinding 500N	670.34	591.94	609.61	565.5
Grinding 750N	1056.17	865.17	916.97	886.95

Legends to the Figures

Fig. 1: Left AMSJI with color-coded components

Fig. 2: Von Mises stress [MPa] distribution in the left AMSJI in the case of an average occlusion of 200 N. Maximal stress is indicated by the pink circle.

Fig. 3: Logarithmic strains [-] in the maxilla in the case of average occlusion at the left side of the mouth. Thresholds were set to 50 - 1500 με.

Fig. 4: Logarithmic strains [-] in the maxilla in the case of maximal occlusion at the left side of the mouth. Thresholds were set to 50 - 1500 με.

Fig. 5: Von Mises stress [MPa] in the left AMSJI in the case of a maximal clenching force of 1000 N. Maximum stress is indicated by the pink circle.

Fig. 6: Von Mises stress [MPa] in the implant structure in the case of a maximal grinding force of 500 N. Peak values indicated by colored circles.

Fig. 7: Logarithmic strains [-] in the maxilla in the case of a maximal grinding force of 500 N. Thresholds were set to 50 - 3000 με.

Figure 1

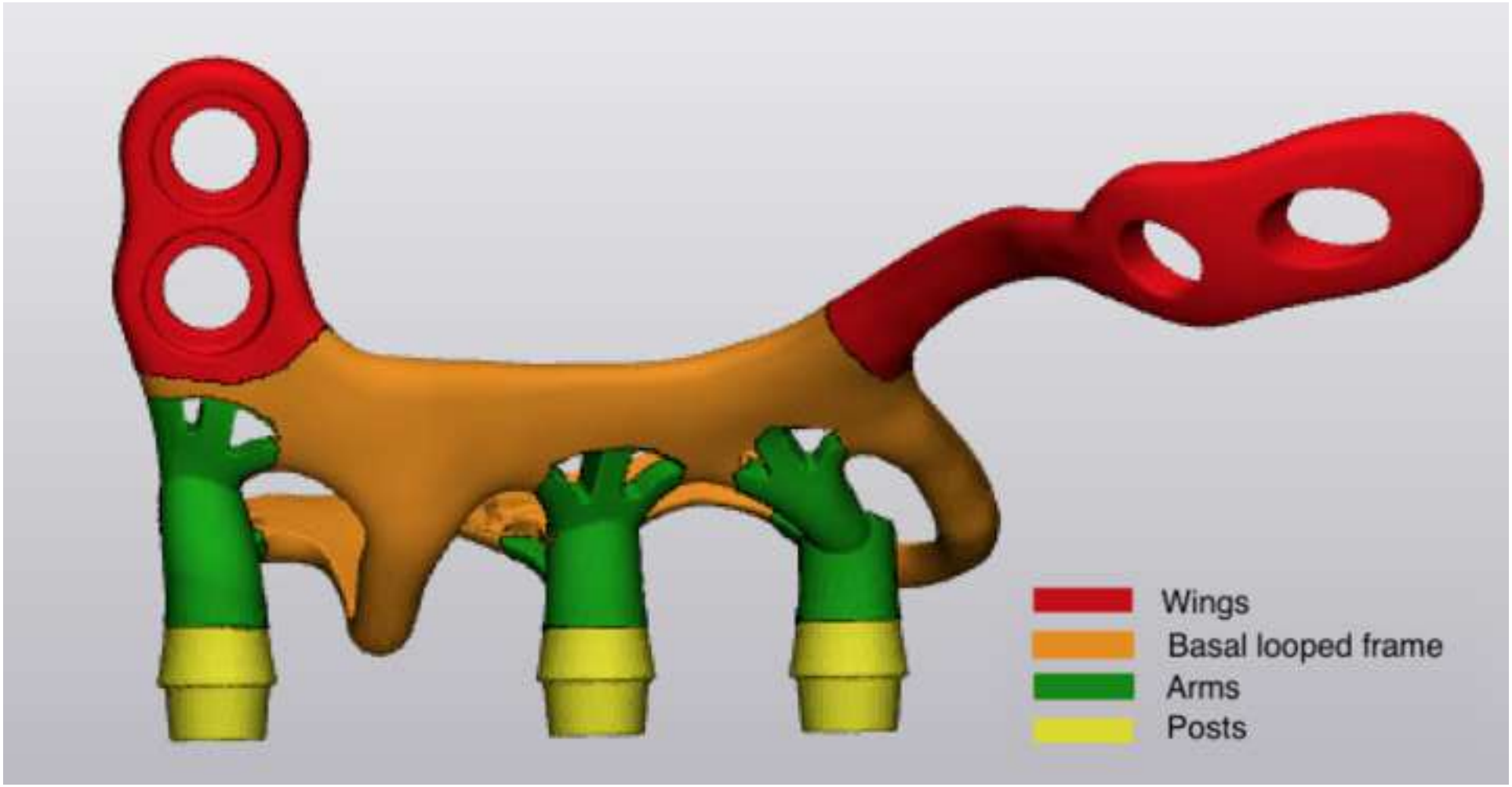

Figure 2

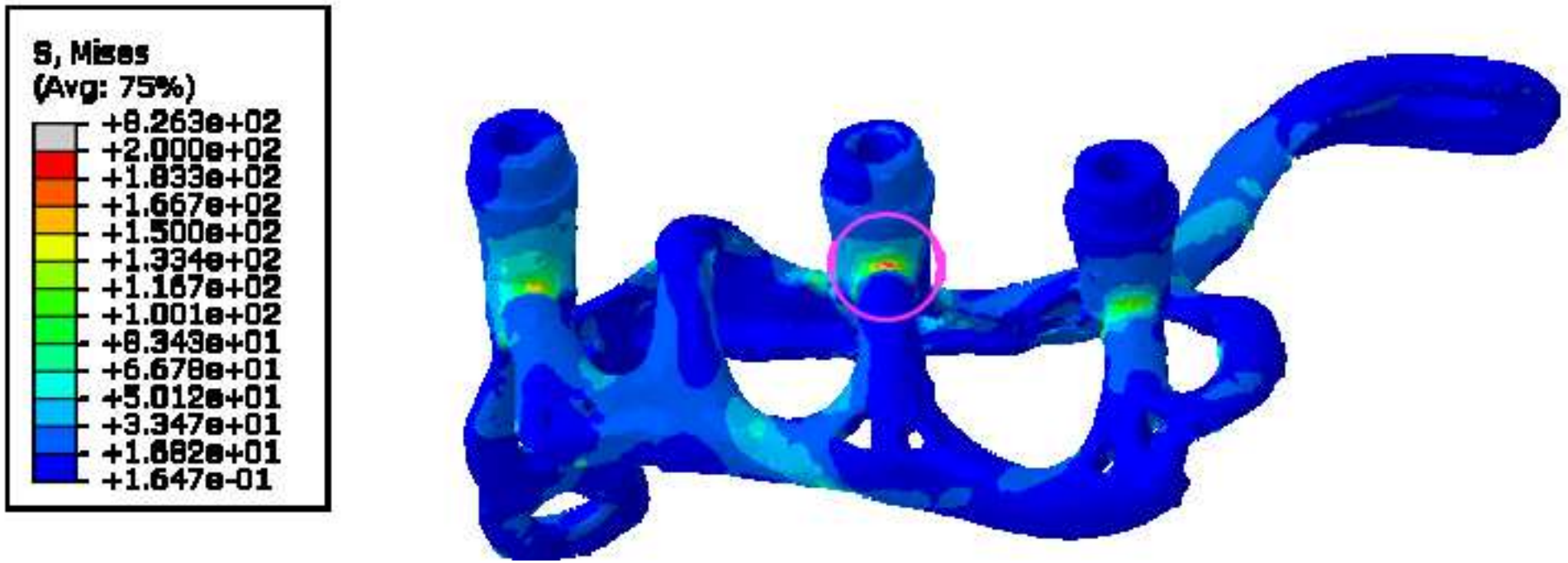
S, Mises
(Avg: 75%)
+8.263e+02
+2.000e+02
+1.833e+02
+1.667e+02
+1.500e+02
+1.334e+02
+1.167e+02
+1.001e+02
+8.343e+01
+6.678e+01
+5.012e+01
+3.347e+01
+1.682e+01
+1.647e-01

Figure 3

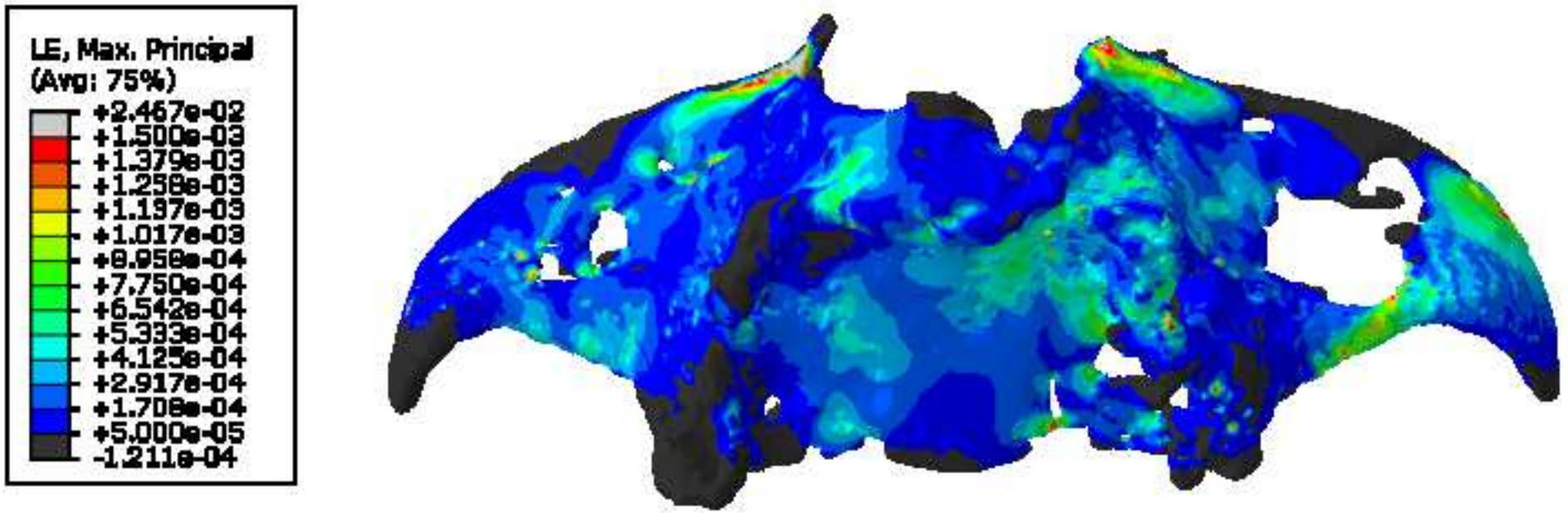
LE, Max. Principal
(Avg: 75%)
+2.467e-02
+1.500e-03
+1.379e-03
+1.258e-03
+1.137e-03
+1.017e-03
+8.958e-04
+7.750e-04
+6.542e-04
+5.333e-04
+4.125e-04
+2.917e-04
+1.708e-04
+5.000e-05
-1.211e-04

Figure 4

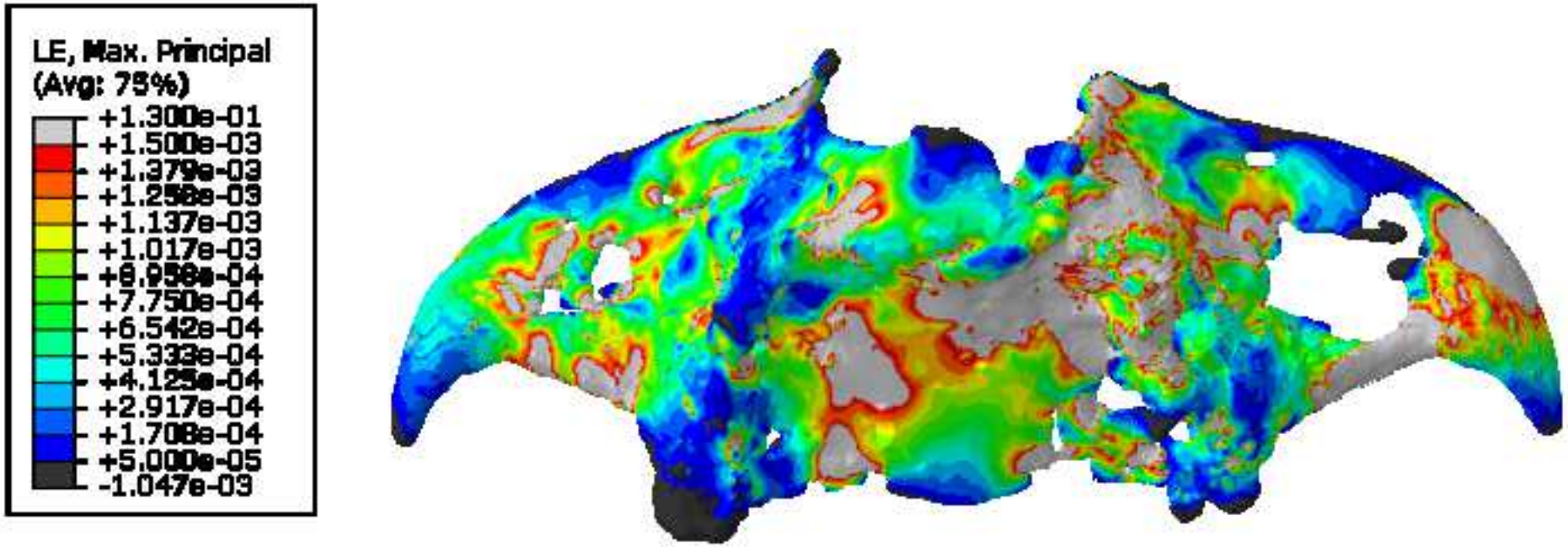
LE, Max. Principal
(Avg: 75%)
+1.300e-01
+1.500e-03
+1.379e-03
+1.258e-03
+1.137e-03
+1.017e-03
+6.958e-04
+7.750e-04
+6.542e-04
+5.333e-04
+4.125e-04
+2.917e-04
+1.708e-04
+5.000e-05
-1.047e-03

Figure 5

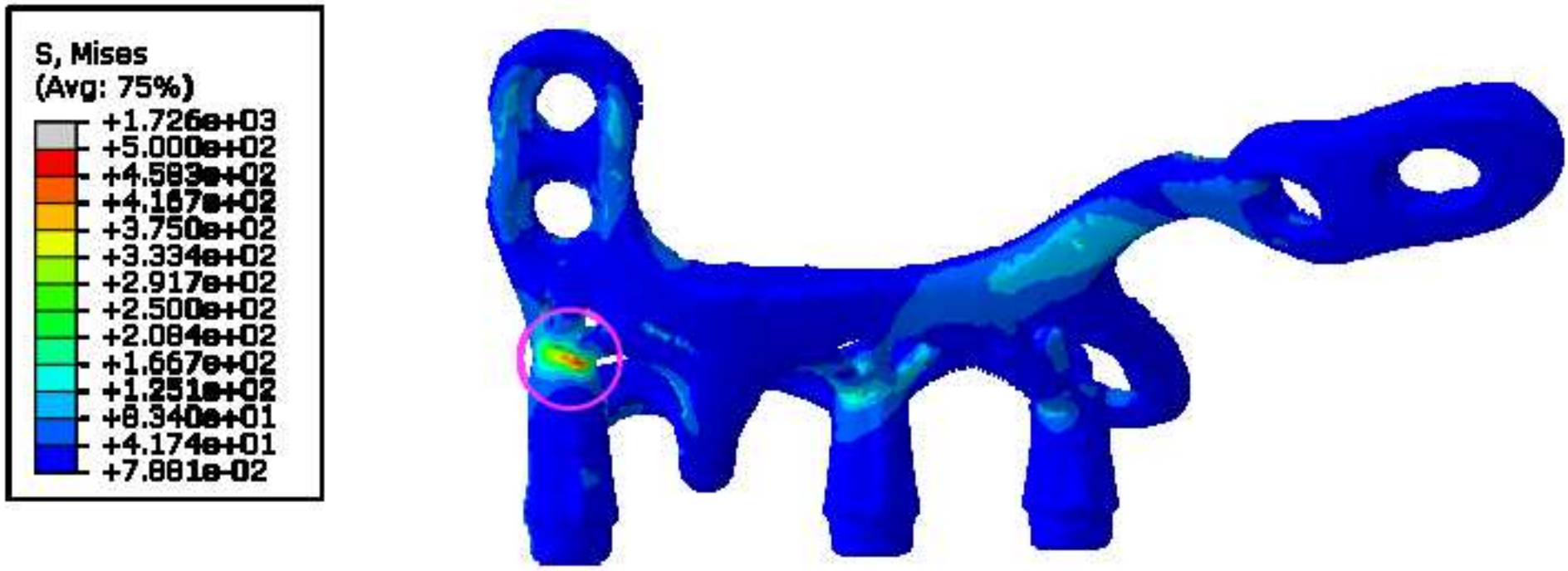
S, Mises
(Avg: 75%)
+1.726e+03
+5.000e+02
+4.583e+02
+4.167e+02
+3.750e+02
+3.334e+02
+2.917e+02
+2.500e+02
+2.084e+02
+1.667e+02
+1.251e+02
+8.340e+01
+4.174e+01
+7.881e-02

Figure 6

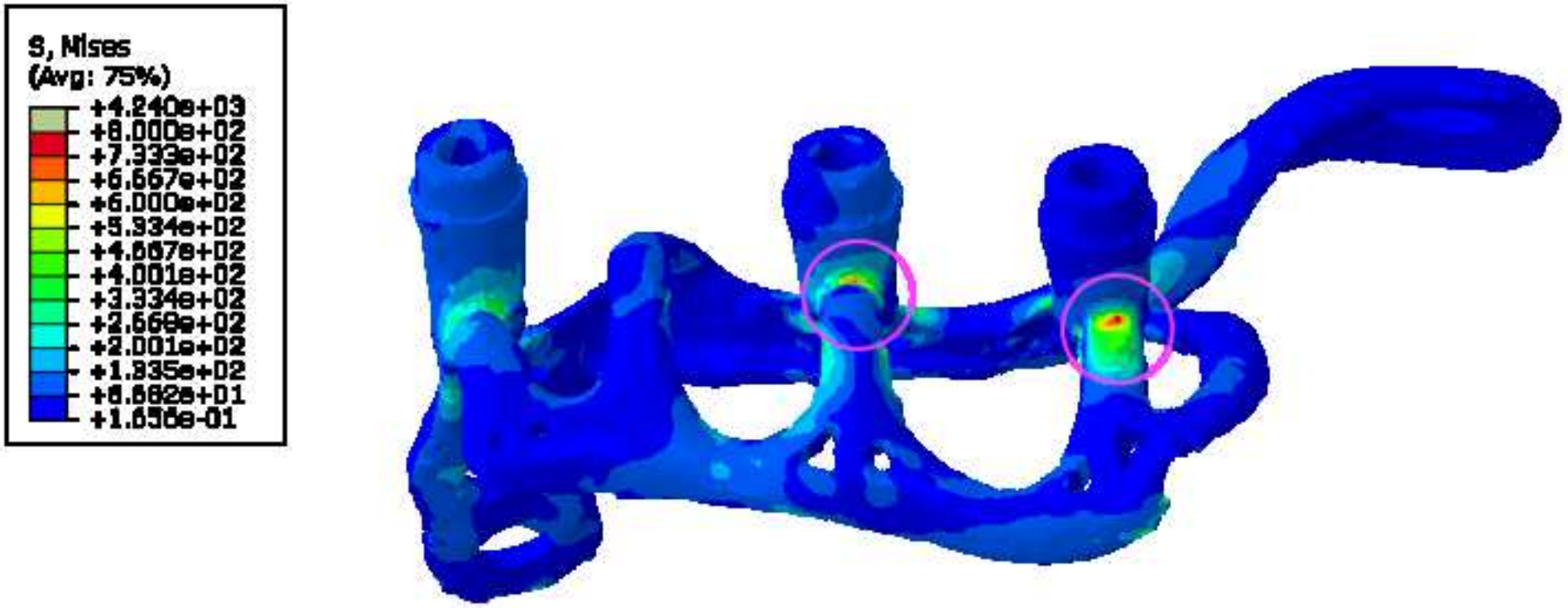
S, Mises
(Avg: 75%)
+4.240e+03
+8.000e+02
+7.333e+02
+6.667e+02
+6.000e+02
+5.334e+02
+4.667e+02
+4.001e+02
+3.334e+02
+2.668e+02
+2.001e+02
+1.335e+02
+6.682e+01
+1.636e-01

Figure 7

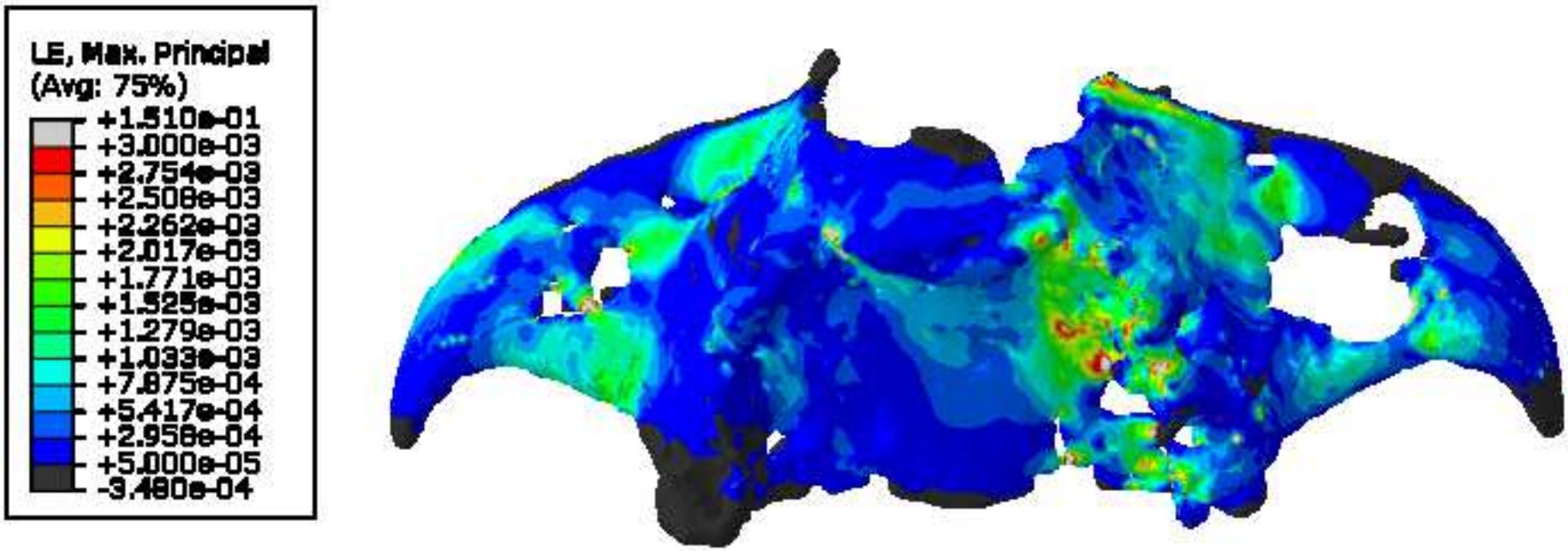
LE, Max. Principal
(Avg: 75%)
+1.510e-01
+3.000e-03
+2.754e-03
+2.508e-03
+2.262e-03
+2.017e-03
+1.771e-03
+1.525e-03
+1.279e-03
+1.033e-03
+7.875e-04
+5.417e-04
+2.958e-04
+5.000e-05
-3.480e-04